# Validation of the TWOPORFLOW code for the core analysis of liquid metal-cooled reactor with selected experiments

Wenpei Feng [a],[*], Uwe Imke [b], Kanglong Zhang [b], Victor Sanchez-Espinoza [b], Hongli Chen [a],[*]

[a] *School of Nuclear Science and Technology, University of Science and Technology of China, Hefei 230026, China*
[b] *Karlsruhe Institute of Technology, Institute for Neutron Physics and Reactor Technology, Hermann-von-Helmholtz-Platz 1, D-76344 Eggenstein-Leopoldshafen, Germany*

## ABSTRACT

TWOPORFLOW (TPF) is a thermal–hydraulic code that utilizes a porous medium approach in three-dimensional Cartesian coordinates. It can simulate the flow phenomenon in fuel assemblies or reactor cores by solving three conservation equations (single-phase) or six conservation equations in a two-fluid liquid–vapor approach. Many constitutive correlations e.g. pressure loss, interfacial friction, and heat transfer (wall, liquid–vapor interface), are included to close the system of equations. The code was recently extended to simulate pre-Critical Heat Flux (CHF) and CHF heat transfer relevant for Boiling Water Reactor (BWR). In this paper, the code's simulation capability for liquid metal-cooled reactors core is validated using three experimental data sets: pressure drop of the 19-pin rod in THEADES LBE loop, the BREST-type reactor benchmark problem, and the NACIE-UP Block Fuel Pin Simulator (BFPS) test. The results show that TPF can be used not only for square rod bundle arrangements but also for hexagonal arrangements; the code can reasonably predict the thermal–hydraulic behavior of liquid metal-cooled reactors under normal and off-normal conditions.

## 1. Introduction

Over the past several decades, various thermal–hydraulic codes (Cao et al., 2019; Imke et al., 2010; Kondo et al., 1992; Liu and Scarpelli, 2015; Sanchez et al., 2010; Teschendorff et al., 1997) are developed to analyze the behavior of Lead Fast Reactors (LFR). They can be divided into the system-, sub-channel-, and Computational Fluid Dynamic (CFD)-codes according to different simulation capabilities, numerical approaches, and spatial computational domains. The system thermal-–hydraulic codes describe the stationary or dynamic behavior of the overall nuclear power plant using mainly 1D or coarse mesh 3D models. While the majority of the quasi-3D sub-channel codes focus on the core behavior at the subchannel level (spatial discretization) including crossflow among neighbor subchannels, it is assumed that any lateral flow through the gap region between sub-channel loses its sense of direction after leaving the gap region which means that some lateral flow phenomena are ignored. CFD codes are general codes with flexible spatial discretization where the mesh size may heavily depend on the physical problem to be solved and the type of analysis to be done (Large Eddy Simulation (LES), Reynolds-Averaged Navier-Stokes (RANS), Direct Numerical Simulation (DNS)). However, a proper spatial resolution of a complex 3D-geometry, e.g., a fuel assembly for a CFD simulation, may require an enormous number of fine meshes. Hence, the detailed analysis of a reactor core is nowadays impracticable due to the huge problem size and subsequent CPU consumption.

Hence, an alternative solution is the use of 3D porous media codes such as PORFLO (Ilvonen et al., 2014), CUPID (Yoon et al., 2014), TWOPORFLOW (Imke, 2004).

In the Karlsruhe Institute of Technology (KIT), researchers focus on the development, improvement, and validation of TPF (Jauregui Chavez et al., 2018). In this context, the validation process (V&V) for any numerical code for safety evaluations is very important and it depends on available experimental data for safety-relevant phenomena of the reactor type under discussion. Recently, TPF was validated against the BWR Full-size Fine-mesh Bundle Test (BFBT) benchmark. The obtained results showed that TPF has satisfactory accuracy in predicting the BWR thermal–hydraulic behavior (Chavez et al., 2018). The main objective of this study is to validate TPF using experimental data and to demonstrate its appropriateness for the analysis of liquid metal-cooled reactors.

In Chapter 2, a brief description of TPF is given. The validation of TPF using data of three tests is presented and discussed in Chapter 3. Finally, Chapter 4 gives a summary and proposes future work.

## 2. Brief description of TPF

TPF (Chavez et al., 2018; Imke, 2004) is a transient analysis code for three-dimensional, single- and two-phase flows in rod bundles or LWR-cores. Steady-state problems are solved using a pseudo-transient approach. Mass, momentum, and energy conservation equations are solved for a 3D cartesian geometry. A semi-implicit numerical procedure based on the implicit continuous Eulerian method is used to solve the conservation equations with a finite volume method using a staggered mesh scheme. The code is based on a porous media approach which means that the solid structure such as rod bundles are simplified as blocked volumes and areas in the flow region. Users need to set the porosity parameters for the flow field and the number of rods per cell for the rod heat transfer. Like other coarse mesh thermal–hydraulic codes, the primary strategy for TPF is to calculate the average of the required thermal–hydraulic parameters in each subchannel. It permits to predict safety-relevant phenomena like void fraction, pressure drops, cladding and fuel temperature, critical heat flux, etc.

## 3. Validation of TPF using experimental data

In this paper, the validation of TPF for liquid metal cooled fast reactor is the main purpose. Hence, relevant experimental data publically available for the research community is identified for code validation. Some examples of relevant experiments are e.g. the ORNL-19 (Fontana et al., 1973), NACIE-UP Block Fuel Pin Simulator (BFPS) (Ivan DI PIAZZA, 2018), BREST-type reactor benchmark (Carlsson and Wider, 2005), THEADES loop(Pacio et al., 2014), etc. Some of them are selected for the validation of TPF. The pressure drop analysis of the 19-pin bundle of THEADES loop is selected for the validation of the wall friction model. In addition, the BREST-type reactor benchmark and the NACIE-UP BFPS experiment are selected for the assessment of simulation accuracy of TPF under different geometries (square lattice or hexagonal arrangement) and working conditions (unblocked and blockage accident).

### 3.1. Pressure drop models in TPF

In TPF, wall friction of the single-phase flow is defined by:

$$F = \left( \frac{f\rho \left| \vec{V} \right|}{2D_h} + P_{ls} \right) \left| \vec{V} \right| \tag{1}$$

$$P_{ls} = \frac{P_{lsc}\rho \left| \vec{V} \right|}{2\Delta x} \tag{2}$$

where:
$D_h$: Hydraulic diameter
$f$ : Wall friction coefficient
$\rho$: Density
$\vec{V}$: Velocity of fluid
$P_{ls}$: Spacers friction factor
$P_{lsc}$: Pressure loss coefficient

The single-phase flow Darcy Weisbach friction coefficient $f$ is taken from Churchill (Churchill and SW, 1977)

$$f = 8 \left[ \left( \frac{8}{\text{Re}} \right)^{12} + \frac{1}{(a+b)^{\frac{3}{2}}} \right]^{\frac{1}{12}} \tag{3}$$

$$a = \left[ 2.457\ln \left( \frac{1}{\left( \frac{7}{\text{Re}} \right)^{0.9} + 0.27 \frac{\epsilon}{D_h}} \right) \right]^{16} \tag{4}$$
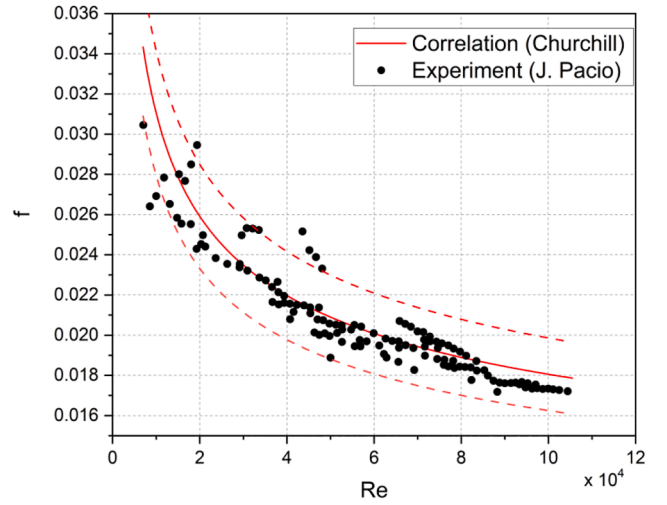


**Fig. 1.** Comparison of Churchill model with experimental data in the validation of pressure drop. The solid line refers to the correlation of Churchill and the dash-dot lines the deviation of ± 10% from it.
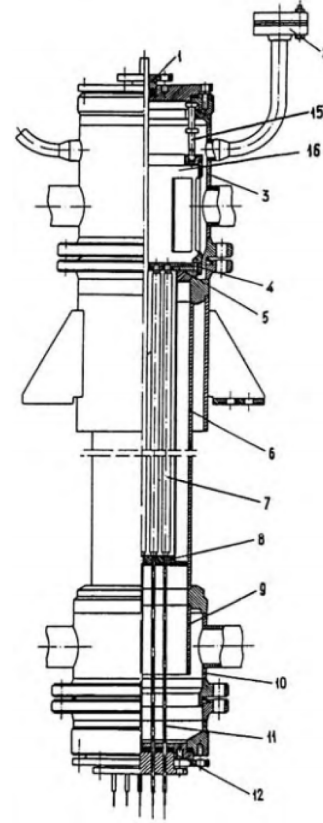


**Fig. 2.** Construction of the model assembly. 1-gasket, 2-thermocouples outlet, 3,10-top and bottom collector, 4-grid of thermocouples, 5,8-bottom and top centering grids, 6-model vessel, 7-pin simulators, 9-guiding vessel, 11-power supplier, 12-power supplier obturating, 13-square wrapper, 14-rotary (measuring) pin simulator, 15-support bolt, 16-vessel.
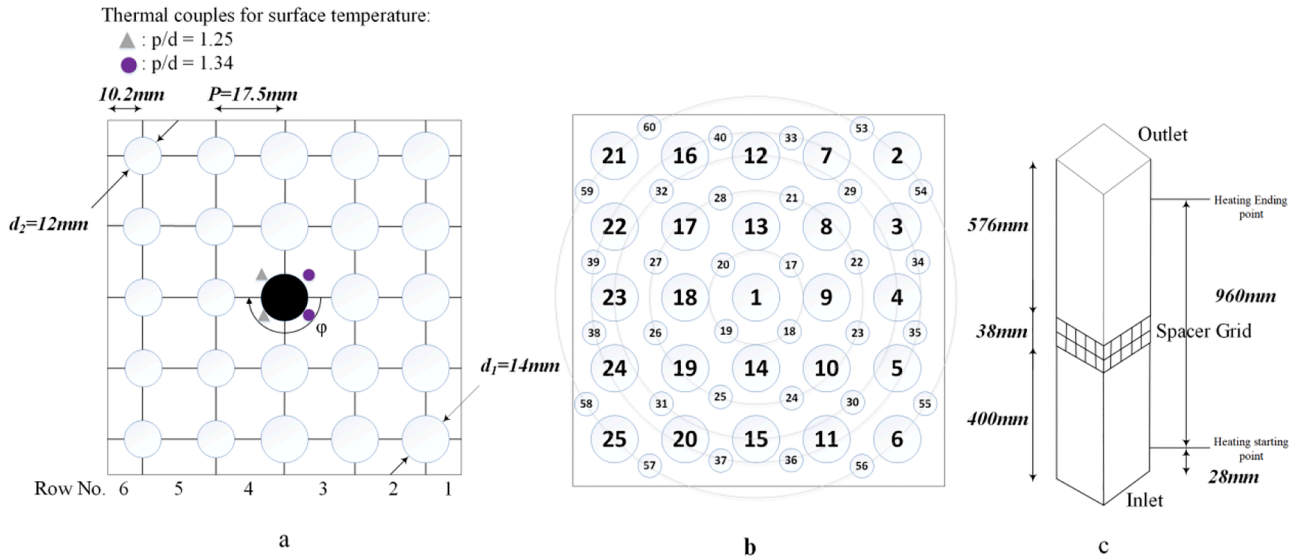
**Fig. 3.** a) Transverse cross-section, b) The scheme of arrangement of pin simulators and thermocouples in coolant channels of the model bundle. 1–25 pin simulators, 17–40, 53–60 thermocouples in the coolant and c) axial view of the experimental fuel assembly.

**Table 1**
Experimental conditions for the five tests.

| Conditions | Tests | | | | |
|---|---|---|---|---|---|
| | 1 | 2 | 3 | 4 | 5 |
| Inlet velocity (m/s) | 2.6 | 2.6 | 2.6 | 2.6 | 2.6 |
| Inlet temperature (°C) | 55.84 | 59.21 | 62.67 | 60.52 | 58.05 |
| Pin power$_{d=14mm}$ (W) | 1.35 | 1.65 | 2 | 2 | 2 |
| Pin power$_{d=12mm}$ (W) | 2 | 2 | 2 | 1.65 | 1.35 |

$$b \quad \left[\frac{37530}{Re}\right]^{16} \tag{5}$$

If the Reynolds number is less than 100 the laminar flow formula is taken due to numerical reasons with the large exponent in variable b:

$$f \quad \frac{64}{Re} \tag{6}$$

For user convenience, local pressure losses for example by grid spacers in TPF are defined by a pressure loss coefficient given by input.

Fig. 1 shows the comparison between the correlation adopted in TPF and the experimental data of J.Pacio et al. (Pacio et al., 2014). Good agreement between the experimental data and predicted values is found, most of the values are within ± 10%.

### 3.2. The BREST-type reactor benchmark problem

The general objectives of this benchmark problem (Carlsson and Wider, 2005) are to analyze thermo-hydraulic characteristics of a bundle cooled by liquid metal and to estimate the reliability and accuracy of thermohydraulic codes. The experiments were performed on assembly (see Fig. 2) cooled by the liquid alloy of 22% sodium and 78% potassium.

Experimental studies are carried out using a non-uniform model (see Fig. 3) which consists of 25 pin simulators with a square arrangement of pins located into the square wrapper. There are two zones with different pitch-to-diameter ratio $p/d_1$  1.25 and $p/d_2$  1.46 ($d_1$  14 mm, $d_2$  12 mm). The total length of the fuel elements is 1,014 mm, of which the heated length is 960 mm, and the lower boundary of the heated region is 28 mm above the inlet. Pin simulators are spaced by the bottom and top centering grids and by transverse grid spacer located from the inlet at a distance of 38 mm.
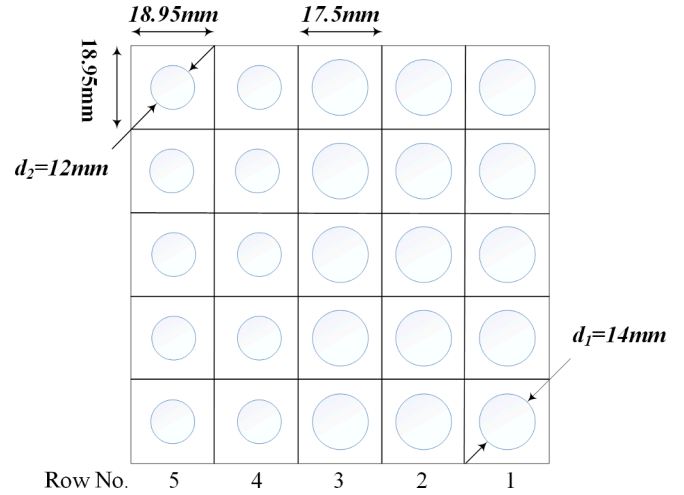


**Fig. 4.** Mesh of the TPF model for the BREST-type reactor.

The measuring pin (central pin) was allowed to rotate in the packing gland. On the surface of the measuring pin, 12 thermocouples (THC) are located in the longitudinal grooves and placed with azimuth spacing Δφ 30 °C. The non-measuring pin simulators were stationary.

The coolant temperature at the exit from the assembly was measured in all cells of the model using THC in protective capillaries, mounted in the thermal array (see Fig. 3b), and inserted into the cell when it is placed on the top end lattice.

Five tests are performed for the specific conditions of Table 1, where the coolant inlet temperature and the pin power were varied. The flow rate is fixed and so is the Reynold number and Pelect number, which are around 53,393 (Re) and 1,316 (Pe), respectively. In this study, conditions 1–3 is calculated and compared with the experiments.

### 3.2.1. TPF model of the BREST-type reactor pin simulator

In general, TPF allows a flexible representation and discretization of the computational domain e.g, centered rod, centered coolant, or assembly-wise approach. However, in the case of a non-uniform assembly, as is the case for one of the BREST-type reactors, TPF can be only discrete in a centered rod scheme (Fig. 4), where a 5 × 5 sub-channels arrangement can be observed with 52 axial cells. The number of rods

**Table 2**
Physical properties of eutectic 78%K + 22%Na alloy (0–200 °C) (T in °C).

| Property | Correlation | | Units |
|---|---|---|---|
| Density | $\rho$ | $880.1 - 0.27 \cdot T$ | kg/m³ |
| Heat Capacity | $C_p$ | $974.92 - 0.42 \cdot T + 0.002 \cdot T^2$ | J/(kg·K) |
| Heat Conductivity | $\lambda$ | $22.368 - 0.0088 \cdot T + 0.00156 \cdot T^2$ | W/(m·K) |
| Dynamic Viscosity | $\mu$ | $(807.162 - 4.2497 \cdot T + 0.0094 \cdot T^2) \cdot 10^{-6}$ | Pa·s |

per channel is 1.0.

Since coolant data obtained by simulation and experiment do not correspond to each other, the experimental data needs to be simply interpolated for a consistent comparison with the predicted data according to the TPF meshing. In this study, the TPF mesh (consists of 5 rows, see Fig. 4) is regarded as the target mesh, and the experimental data (experimental results were arranged in 6 rows, see Fig. 3a) is regarded as the source field, interpolation can be expressed according to the following formula:

$$\text{Row5}_{\text{target}} = 0.5 \times (\text{Row6}_{\text{source}} + \text{Row5}_{\text{source}}) \tag{7}$$

$$\text{Row4}_{\text{target}} = 0.5 \times (\text{Row5}_{\text{source}} + \text{Row4}_{\text{source}})$$

$$\text{Row3}_{\text{target}} = 0.5 \times (\text{Row4}_{\text{source}} + \text{Row3}_{\text{source}})$$

$$\text{Row2}_{\text{target}} = 0.5 \times (\text{Row3}_{\text{source}} + \text{Row2}_{\text{source}})$$

$$\text{Row1}_{\text{target}} = 0.5 \times (\text{Row2}_{\text{source}} + \text{Row1}_{\text{source}})$$

The material properties for the TPF input are depicted in Table 2. Thermophysical properties have an accuracy of ± 5% as reported by (Orlov et al., 2004).

The blockage cross-section caused by the spacer grid is about 20%. According to Rheme's (Rehme, 1978) study, the pressure loss caused by grid spacers are calculated based on this formulation:

$$\Delta P_S = C_v \left(\frac{A_s}{A_v}\right)^2 \frac{1}{2} \rho V^2 = K \frac{1}{2} \rho V^2 \tag{8}$$

where

$C_v$: drag coefficient
$A_v$: cross-section area without grid spacer
$A_s$: cross-section area with grid spacer
$K$: loss coefficient of grid spacer

The turbulence mixing coefficient is set to 0.01. The correlation (Zhukov et al., 1994) for heat transfer to the coolant is set as an input:

$$\text{Nu} = 7.55 \frac{P}{D} - 14 \left(\frac{P}{D}\right)^{-5} + 0.007 \cdot Pe^{\left(0.64 + 0.246 \frac{P}{D}\right)} \tag{9}$$

where:
P: rod pitch
D: rod diameter
Pe: Peclet number

### 3.2.2. TPF simulations and discussion of results

The conditions 1–3 in Table 1 were analyzed with TPF using the boundary conditions at the bundle inlet (mass flow rate, coolant temperature) and the bundle outlet (pressure) as well as the power per pin. The same spatial nodalisation of the bundle is used for all simulations.

Since TPF does not have a steady-state solution as many other codes e.g. COBRA-IV, a transient simulation is performed where the boundary conditions are kept constant as indicated in Table 1. TPF has an
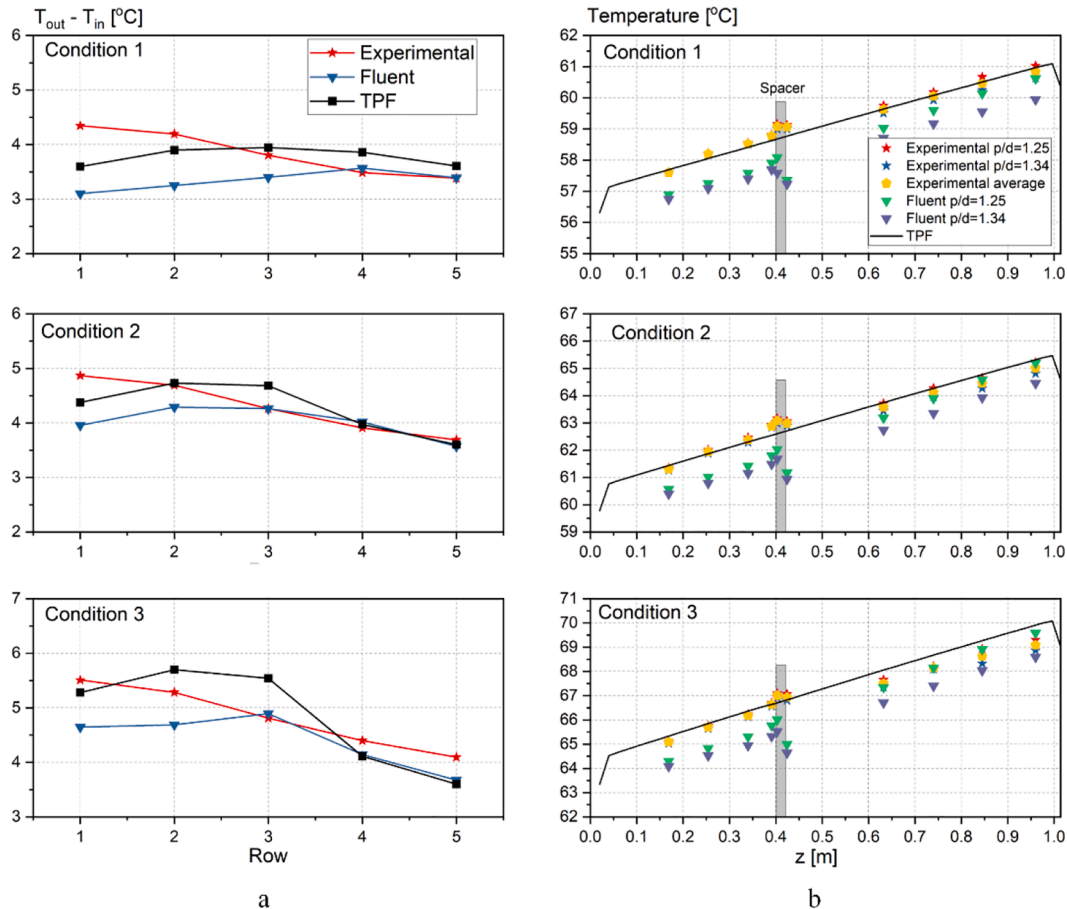


**Fig. 5.** a) Average coolant heating at the outlet from the model assembly and b) surface temperature of the measuring fuel rod simulator along with the height.

| Identifier | $N_{15}/N_{10}$ (kW/kW) | $\bar{\varepsilon}_{rel}$[%](Coolant Temperature) | | $\bar{\varepsilon}_{rel}$[%](Cladding Temperature) | |
|---|---|---|---|---|---|
| | | TPF | Fluent | TPF | Fluent |
| 1 | 1.35/2.00 | 9.062 | 12.882 | 0.243 | 1.597 |
| 2 | 1.65/2.00 | 4.965 | 6.677 | 0.365 | 1.409 |
| 3 | 2.00/2.00 | 9.174 | 8.961 | 0.523 | 1.266 |

| Parameter | Value |
|---|---|
| External cladding diameter (mm) | 10 |
| Rod pitch (mm) | 14 |
| Duct width (mm) | 62 |
| Bundle length (mm) | 800 |
| Active length (mm) | 600 |
| Inlet region length (mm) | 355 |
| Mixing region length (mm) | 575 |
| Number of pins | 19 |

slightly with power increasing. Therefore, it can be concluded that the results of coolant heating obtained with the TPF is sensitive to the energy release along the subzones. The same phenomenon is captured in Ref. (Afremov et al., 2004; Carlsson and Wider, 2005; Ohshima and Imai, 2004; Pena and Esteban, 2004; Son and Suh, 2004). In contrast, the experimental result is more sensitive to the geometry of the assembly, with the coolant temperature always higher in the cells formed by large-diameter simulators. For the results calculated with the FLUENT code, it describes well with the experimental data in the central zone of the model assembly in all regimes but strong discrepancies are observed at the periphery.

In Fig. 5b, the simulated and experimental axial temperatures on the center pin surface are shown. Two values are obtained simultaneously in the same axial position from the experiment (see Fig. 3). One is from the region where pitch-to-diameter is 1.25, and the other is from where pitch-to-diameter is 1.34. However, since TPF only calculates an average temperature in each axial location, the results from the experiments are averaged into a single value in each axial location. It can be concluded that the prediction values of TPF agree well with the experimental data;

The relative error from the experimental data was calculated and it is shown in Table 3. The reported accuracy of the experimental values has been estimated of about 10%. One can see that the coolant temperature rise calculated with TPF has an accuracy smaller than 10%, while the cladding temperature is calculated with an accuracy of around 0.5%.

### 3.3. The NACIE-UP BFPS test section

The flow blockage accident in a fuel sub-assembly is considered one of the main issues in the fourth-generation heavy liquid metal-cooled reactors. Particularly for Lead Fast Reactors (LFR), this is also one of the most critical and realistic accidents since lead-alloy is very corrosive to the structural steels (Feng et al., 2020). To study the local and bulk effects of an internal blockage, ENEA (Italian National Agency for New Technologies, Energy and Sustainable Economic Development) designed and built a Blocked Fuel Pin Simulator (BFPS) test section (Ivan DI PIAZZA, 2018) in the NACIE-UP (NAtural CIrculation Experiment UPgrade) facility loop.

The schematic diagram of NACIE-UP is shown in Fig. 6. The primary circuit of the facility is filled with LBE (lead–bismuth eutectic), and is divided into two vertical pipes, working as riser and downcomer, two horizontal pipes, and an expansion tank; A fuel simulator with a maximum power of 250 kW is installed at the bottom of the riser, which will be replaced by the BFPS test section. A shell and a tube heat exchanger is placed at the upper part of the downcomer, and the secondary side is filled with water at 16 bars.

The tests are performed in an assembly (geometrical data in Table 4, sketch in Fig. 7) consisting of a 19-pin triangular bundle in a hexagonal wrapper, which is spaced using two grid-spacers on both sides of the active length.

During the experiments, Pins 1, 2, 5, 15 are instrumented with wall embedded thermocouples (blue mark in Fig. 7b), and sub-channel B2 is instrumented with bulk thermocouples marked in orange. The measurements took place at the different axial levels of $z$ 10, 20, 30, 40, 50, 60, 70, 80, 90, 100, 150, 200, 300, 400, 500, 600 mm above the
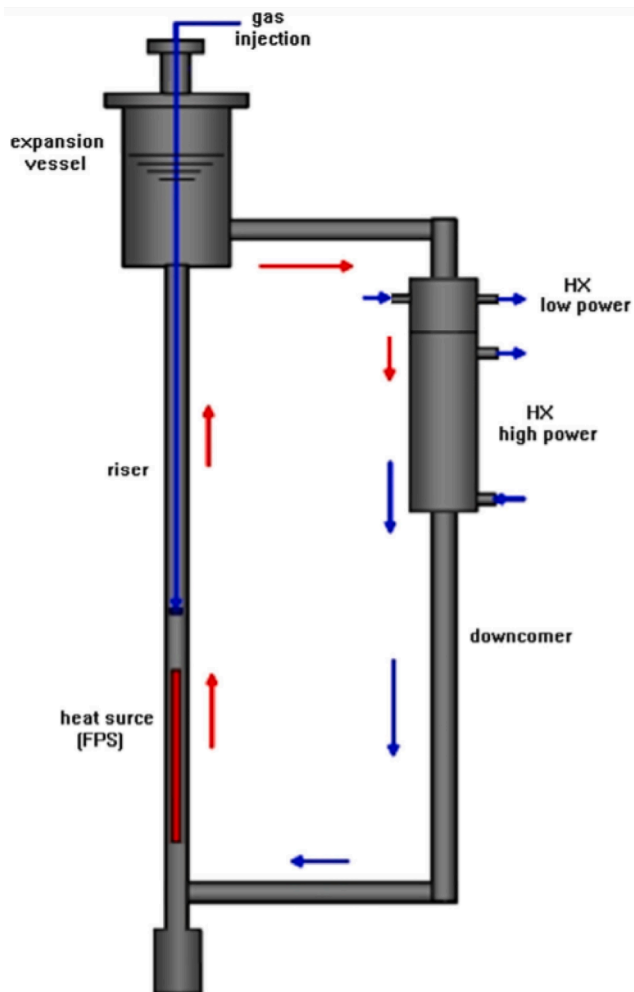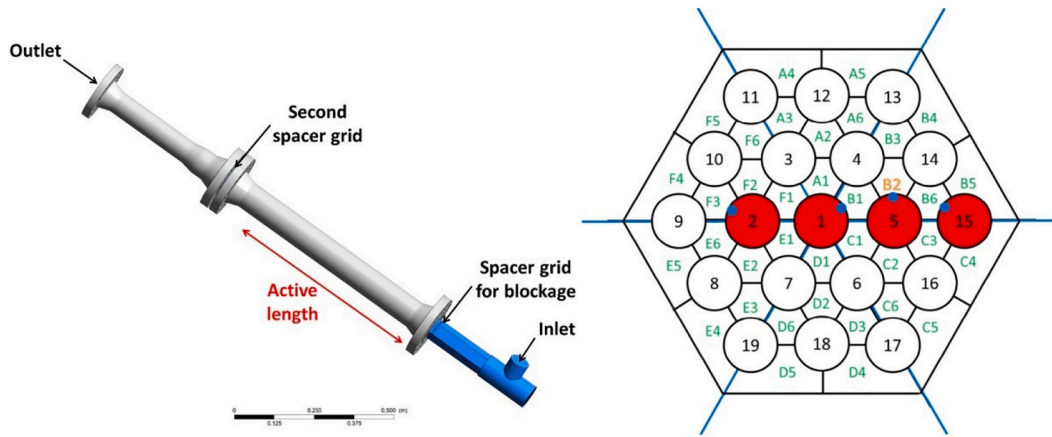


**Fig. 6.** Schematic diagram of the NACIE-UP facility.

automatic timestep algorithm and the calculation is terminated when the maximum local relative temperature change of the fuel, cladding, and coolant between two-time steps is lower than $10^{-6}$ and the maximum relative pressure change is less than $10^{-7}$.

In Fig. 5a, the simulated and experimental temperature rises of the coolant in each row are compared. The results of fluent are taken from the Ref. (Pena and Esteban, 2004). In the three conditions, the power of the pin $d_1$ 14 mm was increased from condition (1) to condition (3), while the power of the pin $d_2$ 12 mm was kept constant. However, the temperature distributions measured by the experiment among the three conditions are not that different compared to the TPF, and only the temperature level is rising when power increases. It can be seen that the calculation results of TPF in rows 1, 2, 3 show a larger change when increasing the power than the experimental data. Moreover, the calculated temperature of row 4, 5 does not seem to be affected by the power increase in the pins of $d_2$ 12 mm when the measured data increase

**Fig. 7.** BFPS test section; numbering scheme (Marinari et al., 2019) and thermocouples location on the axial plane.
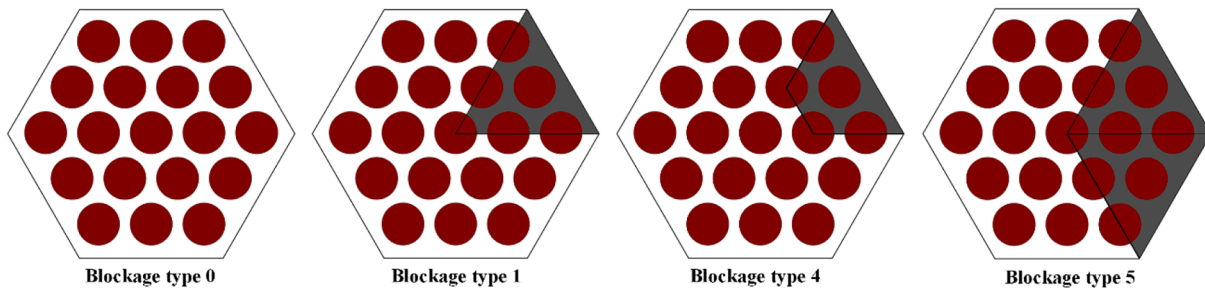


**Fig. 8.** Sketch of the different blockage type simulated.

**Table 5**
Experimental test matrix for BFPS test section.

| Test name | Mass flow rate [kg/s] | Blockage type | $T_{in}$ [°C] | $Q_{nom}$ [kW] | $Q_{eff}$ [kW] |
|---|---|---|---|---|---|
| BFPS − 4-0 | 4.05 | 0 | 222.4 | 24 | 22.8 |
| BFPS − 8-0 | 8.076 | 0 | 263.6 | 48 | 46.25 |
| BFPS −12-0 | 12.45 | 0 | 294.7 | 72 | 70.3 |
| BFPS −14-0 | 18 | 0 | 309.8 | 96 | 92.3 |
| BFPS − 4-4 | 3.75 | 4 | 220.1 | 24 | 22.7 |
| BFPS − 8-4 | 7.97 | 4 | 260.3 | 48 | 46.9 |
| BFPS −10-4 | 10.13 | 4 | 287 | 72 | 70 |
| BFPS − 4-1 | 3.77 | 1 | 223.4 | 24 | 22.82 |
| BFPS − 8-1 | 8.1 | 1 | 259.2 | 48 | 46.68 |
| BFPS −12-1 | 12.62 | 1 | 294.8 | 72 | 70.9 |
| BFPS − 4-5 | 3.65 | 5 | 222.6 | 24 | 23.3 |
| BFPS − 8-5 | 8.15 | 5 | 267.5 | 48 | 46.68 |
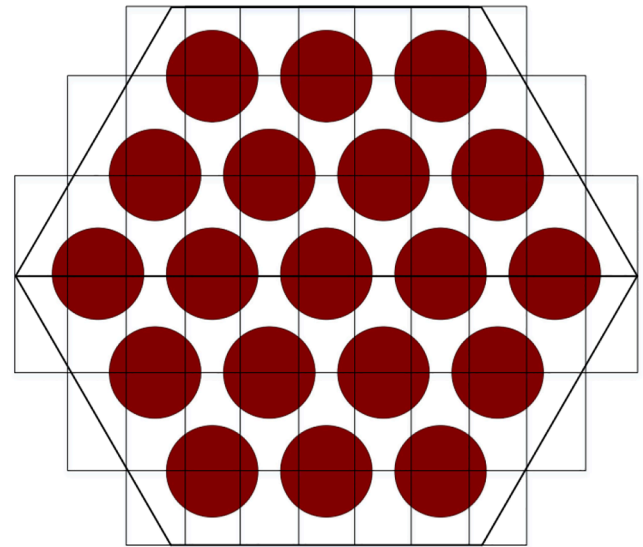


**Fig. 9.** Mesh arrangement in the horizontal plane for the BFPS test section.

According to different mass flow rates and different degrees of blockage (see Fig. 8), the experimental tests are divided into multiple cases (see Table 5). All of them are stationary tests with uniform heating in the pins.

In this study, the active region of tests BFPS-8-0 (no blockage) and BFPS-8-1 (blockage) are simulated with TPF and the predicted parameters are compared with the experimental data and with results of CFD (RANS) simulations from Ref. (Marinari et al., 2019).

beginning of the active region of the pins.

Moreover, the experiment is in stationary condition and each operating condition is run for 5–6 h in a transient state. When the stationary condition is reached, data are collected at a frequency of 1 Hz, the collection time is 20 min to 1 h, and the number of samples is at least 1200 to obtain statistical stable state data. The data were then averaged and the standard deviation of the measurements was smaller than 0.6 °C.

**Table 6**
Physical properties of LBE (T in K).

| Property | Correlation | Units | Maximum Uncertainty | Standard deviation |
|---|---|---|---|---|
| Density | $\rho$  $11065 - 1.293 \cdot T$ | kg/m³ | $\leq 0.8\%$ | 0.58% |
| Heat Capacity | $C_p$  $164.8 - 3.94 \cdot 10^{-2} \cdot T + 1.25 \cdot 10^{-5} \cdot T^2 - 4.56 \cdot 10^{-5} \cdot T^{-2}$ | J/(kg·K) | $\leq 7.0\%$ | 2.4% |
| Heat Conductivity | $\lambda$  $4.94 \cdot 10^{-4} \exp\left(\dfrac{754.1}{T}\right)$ | W/(m·K) | $\leq 6.0\% - 8.0\%$ | 7.2% |
| Dynamic Viscosity | $\mu$  $3.284 + 1.67 \cdot 10^{-2} \cdot T - 2.305 \cdot 10^{-6} \cdot T^2$ | Pa·s | $\leq 10.0\% - 15.0\%$ | 6.2% |
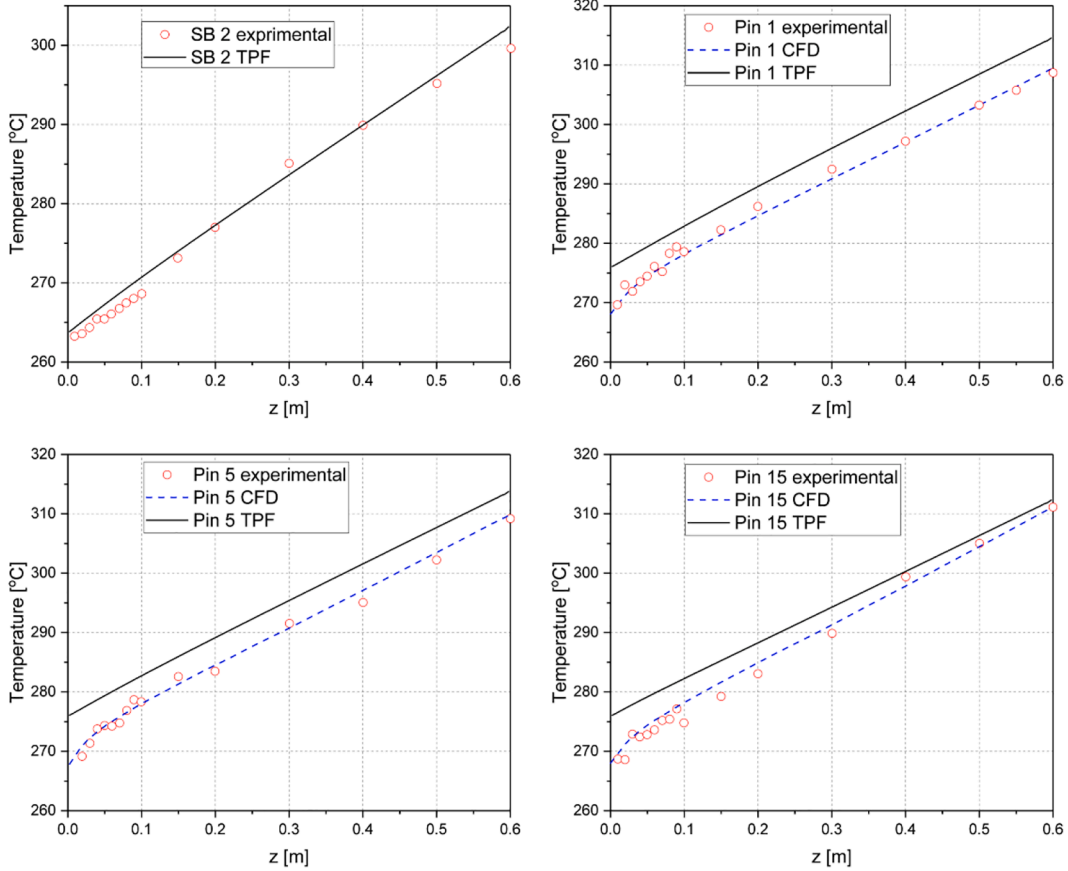


**Fig. 10.** Axial temperature profiles along with the pins and in the B2 channel for case BFPS-8-0.

### 3.3.1. TPF model of the BFPS bundle

Since TPF is based on Cartesian Coordinates, additional work is needed to consistently convert the hexagonal computational domain of the hexagonal fuel assembly to an equivalent Cartesian one. The geometry of the hexagonal assembly is discretized with the Cartesian meshing of TPF as shown in Fig. 9. There, it can be seen that the rods are subdivided into multi virtual rods for each cell. The power fraction of the virtual rods is calculated according to the perimeter ratio. Then, the porosity parameters are calculated using the effective flow area per cell. The heated part is discretized into 100 axial cells. Moreover, the mixing coefficient across the square mesh border of rod bundles with non-mixing spacers is set to 0.03.

The boundary conditions are set according to Table 5, where the effective power of the experiment is considered in calculations. The correlation (Mikityuk, 2009) for heat transfer to the coolant is used

$$\mathrm{Nu} \quad 0.047\left(1 \quad e^{-3.8\left(\frac{P}{D} - 1\right)}\right)\left(\mathrm{Pe}^{0.77} + 250\right) \tag{10}$$

where:
P: rod pitch

D: rod diameter
Pe: Peclet number

The material properties for the TPF input shown in Table 6 are taken from (Marinari et al., 2019). The maximum deviation of the experimental data and standard deviation are reported in addition.

A pseudo transient TPF-calculation is performed for the unblocked test BFPS-8-0 and blocked test BFPS-8-1 with automatic timestep control. Once the convergence criteria of maximum local relative temperature change of the fuel, cladding, and coolant between two-time steps is less than $10^{-6}$ and the maximum relative pressure change less than $10^{-7}$ are achieved, the simulation will be terminated.

### 3.3.2. TPF simulations and discussion of results

In Fig. 10, the experimental axial cladding temperature along with the pin height and the coolant temperature of the subchannel B2 for BFPS-8-0 are compared with the values predicted by TPF. In addition, CFD results are also included in some comparisons when available. Because of the stationary and uniform wall heat flux without any azimuthal variation, a linear profile should be recovered. This phenomenon was reproduced by TPF as shown in Fig. 10, from which one can see
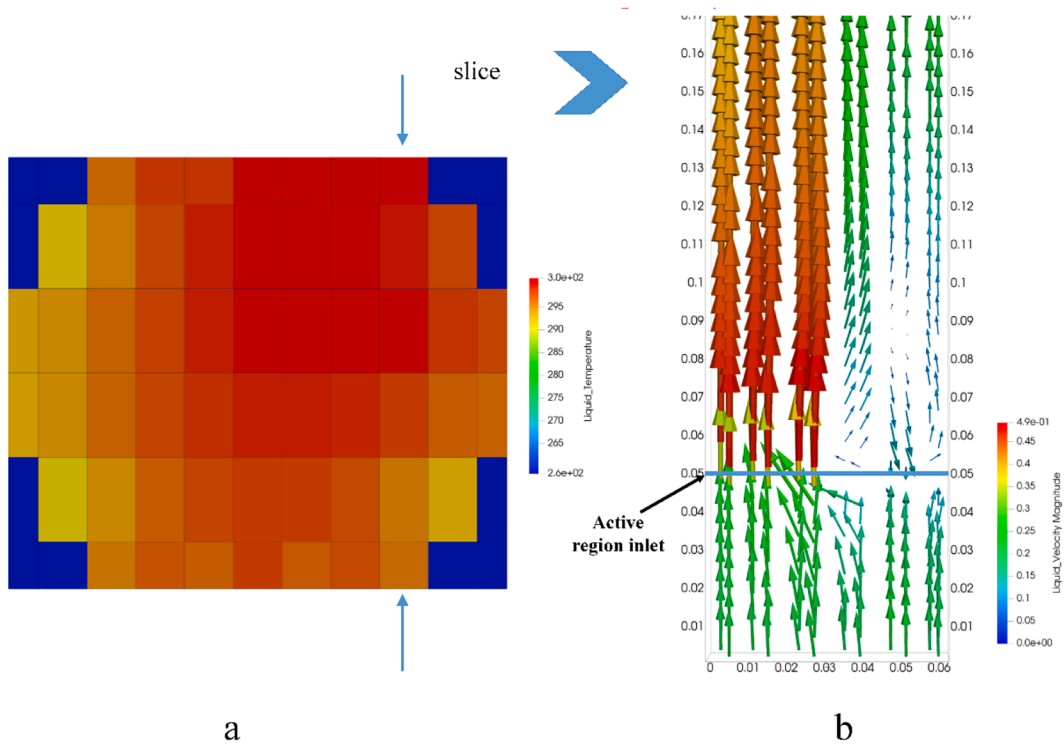
**Fig. 11.** a) outlet liquid temperature and b) velocity vectors behind the blockage in the BFPS-8-1 test case.
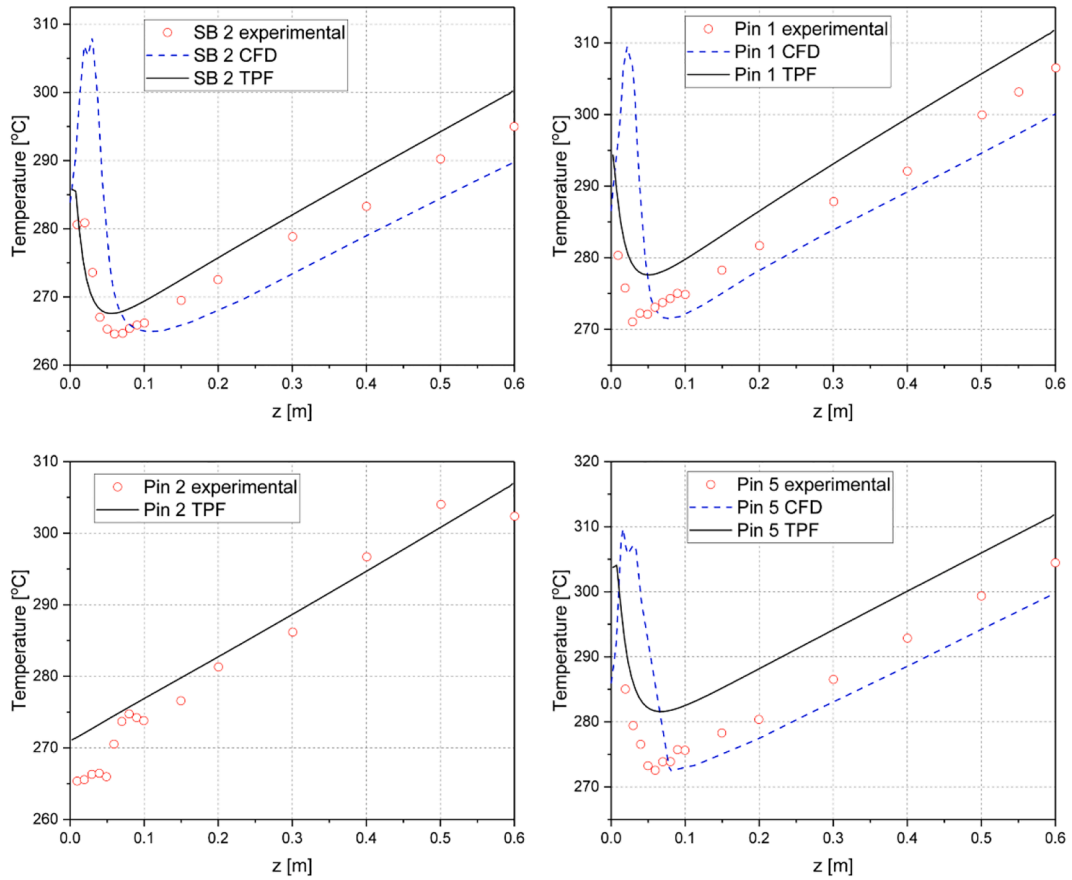


**Fig. 12.** Axial temperature profiles along with the pins and B2 channel for case BFPS-8-1.

the temperature profiles predicted by TPF exhibits a linear trend. The cladding temperature prediction of TPF in pins 1, 5, 15 is a little bit overestimated, especially in the region near the inlet grid spacer, which may be caused due to the absence of grid spacer at the inlet in the TPF model. To summarize the accuracy of the calculation, a root mean square error (RMSE) between the calculation and the measurement is calculated, the values are 1.49, 4.7, 5.21, and 5.46 ℃ for SB2, Pin 1, Pin 5, Pin 15, respectively. The estimated accuracy for the temperature measurement is smaller than 0.6 ℃.

For the blockage test BFPS-8-1, due to the obstacle, a vortex will form behind the blockage region and will deviate locally from the linear profile and reach a maximum deviation at the stagnation point.

The temperature contours at the assembly outlet and the velocity vector of a slice plane are presented in Fig. 11. It can be seen in Fig. 11a that there is a wide variation of temperatures between different channels as a result of the global effect of the blockage, and the temperature peak appears in the blockage channels due to the lower mass flow rate.

In Fig. 12, the predicted and measured axial cladding temperature along with the pin height and coolant temperature at subchannel B2 for BFPS-8-1 are compared. In subchannel B2, the local coolant temperature peak is observed behind the blockage region due to the vortex generated downstream by the blockage. The TPF-simulations capture this phenomenon well, see Fig. 11b, where a coolant recirculation at the cross-section between $z$ 0.05 m and $z$ 0.09 m can be observed. Beyond the vortex, the temperature drops to a minimum value and then it rises linearly. However, the TPF predicts a slightly smaller recirculation zone than the one seen in the experiment, while the CFD predicts a larger one.

Due to this fact, the position of the local minimum temperature is predicted to be nearer downstream than the experiments. In the experiment, the minimum liquid temperature in subchannel B2 is observed at around 0.06 m, while the TPF predicts the value of 0.05 m. Furthermore, the blockage pins (pin 1 and pin 5) exhibit a similar temperature trend as that of subchannel B2.

The TPF overestimates the pin cladding temperature hotspot behind the blockage region, while CFD simulation largely over-predicts the temperature peak because the steady RANS simulation fails to capture the unsteady vortices generated in the recirculation region by the blockage (Marinari et al., 2019). The temperatures of sub-channel B2 and blocked pins at the end of active length are overestimated in this simulation, while CFD predicted smaller values than the experiment. Besides, the TPF predicts a linear profile in pin 2, which agrees reasonably well with the experiment. A root mean square error (RMSE) between the calculation and the measurement is calculated, the values are 3.76, 5,68, 4.37, and 7.54 ℃ for SB2, Pin 1, Pin 2, Pin 5, respectively.

## 4. Summary and outlook

In this paper, the validation of TWOPORFLOW (TPF) for the thermal–hydraulic analysis of liquid metal-cooled reactor core is described and discussed. The validation demonstrats the capabilities of the models implemented in TPF and their interactions in reproducing the experimental data.

In a first step, validation of the wall friction loss correlation adopted in TPF is carried out against the experimental data of J.Pacio et al. (Pacio et al., 2014). Good agreement between the experimental data and predicted values is found, most of the values are within ± 10%. Furthermore, the code is validated against the experimental data from the BREST-type reactor core simulator. The thermal–hydraulic characteristics of the pin bundle under non-uniform geometrical and thermal conditions is simulated. Results show that the coolant temperature rise is calculated with an accuracy smaller than 10%, while the cladding temperature is calculated with an accuracy of around 0.5%. Results from other codes like BRS-TVS.R, SPIRAL, AQUA, FLUENT, STAR-CD, MATRA, and CFX show a similar quality compared to TPF. Secondly, TPF was validated using experimental data obtained from a test with a hexagonal subassembly of the NACIE-UP BFPS experiments to validate

the capabilities of TPF for an internal blockage of the fuel assembly. The results show that TPF can reasonably well simulate the internal blockage accident. Results using the same tests were published before using the CFD code CFX, optaining a similar quality compared to TPF.

Based on the promising results, TPF will be applied to analyze a complete core of a liquid metal cooled reactor. Last but not least, a standardized interface called ICoCo (Interface for Code Coupling) is being implemented in TPF for potential multi-physics and multi-scale coupling purposes.

*CRediT authorship contribution statement*

**Wenpei Feng:** Conceptualization, Methodology, Investigation, Writing – original draft, Writing – review & editing, Visualization. **Uwe Imke:** Methodology, Writing – original draft, Writing – review & editing, Investigation. **Kanglong Zhang:** Methodology, Writing – review & editing, Investigation. **Victor Sanchez-Espinoza:** Writing – review & editing, Investigation. **Hongli Chen:** Writing – review & editing.

## Declaration of Competing Interest

The authors declare that they have no known competing financial interests or personal relationships that could have appeared to influence the work reported in this paper.

## Acknowledgment

## References

Afremov, D., Smirnov, V., Yashnikov, D., 2004. Calculations using BRS-TVS. R code as part of a standard problem "hydraulics and heat exchange in model rod assemblies with liquid-metal cooling", are including uncertainty analysis. Hydrodynamics and heat transfer in reactor components cooled by liquid metal coolants in single/two-phase, 173-196.

Cao, L., Yang, G., Chen, H., 2019. Transient sub-channel code development for lead-cooled fast reactor using the second-order upwind scheme. Progress in Nuclear Energy 110, 199–212.

Carlsson, J., Wider, H., 2005. Results of calculations of a standard problem - 'Hydrodynamics and heat transfer in a subassembly model cooled by liquid metal coolant'. International Atomic Energy Agency (IAEA) 212–226.

Jauregui Chavez, V.J., Imke, U., Sanchez-Espinoza, V., 2018a. TWOPORFLOW: A two-phase flow porous media code, main features and validation with BWR-relevant bundle experiments. Nuclear Engineering and Design 338, 181–188.

Churchill, S.W., SW, C., 1977. Friction-factor equation spans all fluid-flow regimes.

Feng, W., Zhang, X., Chen, H., 2020. Simulation of oxygen mass transfer in fuel assemblies under flowing lead-bismuth eutectic. Nuclear Engineering and Technology 52 (5), 908–917.

Fontana, M., MacPherson, R., Gnadt, P., Parsly, L., Wantland, J., 1973. Temperature Distribution in a 19-Rod Simulated Lmfbr Fuel Assembly in a Hexagonal Duct (fuel failure mockup bundle 2A): Record of Experimental Data. ORNL-TM-4113.

Ilvonen, M., Hovi, V., Taivassalo, V., 2014. 3D Core Thermal Hydraulics With the PORFLO Code: Turbulence Modeling and Porous Medium With Porosity Steps, 2014 22nd International Conference on Nuclear Engineering. American Society of Mechanical Engineers Digital Collection.

Imke, U., 2004. Porous media simplified simulation of single-and two-phase flow heat transfer in micro-channel heat exchangers. Chemical Engineering Journal 101 (1-3), 295–302.

Imke, U., Sanchez, V., Gomez, R., 2010. SUBCHANFLOW. A new empirical knowledge based subchannel code, Annual meeting on nuclear technology. Documentation, p. 2010.

Ivan DI PIAZZA, R.M., V. Sermenghi, G. Polazzi, 2018. SESAME Deliverable 2.7: BFPS experiments. ENEA.

Jauregui Chavez, V., Imke, U., Jimenez, J., Sanchez-Espinoza, V.H., 2018b. Further development of a thermal-hydraulics two-phase flow tool. Atw Internationale Zeitschrift fuer Kernenergie 63, 401–404.

Kondo, S., Tobita, Y., Morita, K., Shirakawa, N., 1992. SIMMER-III: An advanced computer program for LMFBR severe accident analysis, ANP'92 international conference on design and safety of advanced nuclear power plants.

Liu, X.J., Scarpelli, N., 2015. Development of a sub-channel code for liquid metal cooled fuel assembly. Annals of Nuclear Energy 77, 425–435.

Marinari, R., Di Piazza, I., Tarantino, M., Forgione, N., 2019. Blockage fuel pin simulator experiments and simulation. Nuclear Engineering and Design 353, 110215. https://doi.org/10.1016/j.nucengdes.2019.110215.

Mikityuk, K., 2009. Heat transfer to liquid metal: Review of data and correlations for tube bundles. Nuclear Engineering & Design 239 (4), 680–687.

Ohshima, H., Imai, Y., 2004. Thermal hydraulic analysis of model pin bundle with liquid metal coolant–simulation results of standard problem. Hydrodynamics and heat transfer in reactor components cooled by liquid metal coolants in single/two-phase 188–202.

Orlov, Y., Sorokin, A., Bogoslovskaia, G., Ivanov, E., Malkov, V., Li, N., 2004. Specification of the benchmark problem thermal experiments in the ADS target model. Hydrodynamics and heat transfer in reactor components cooled by liquid metal coolants in single/two-phase, 261.

Pacio, J., Daubner, M., Fellmoser, F., Litfin, K., Marocco, L., Stieglitz, R., Taufall, S., Wetzel, T.h., 2014. Heavy-liquid metal heat transfer experiment in a 19-rod bundle with grid spacers. Nuclear Engineering and Design 273, 33–46.

Pena, A., Esteban, G., 2004. Benchmark problem: hydraulics and heat transfer in the model pin bundles with liquid metal coolant. UPV-EHU calculations. Hydrodynamics and heat transfer in reactor components cooled by liquid metal coolants in single/two-phase, 238-250.

Rehme, K., 1978. The pressure drop of spacer grids in rod bundles of 12 rods with smooth and roughened surfaces. Kernforschungszentrum Karlsruhe GmbH (Germany.

Sanchez, V., Imke, U., Ivanov, A., Gomez, R., 2010. SUBCHANFLOW: a thermal hydraulic sub-channel program to analyse fuel rod bundles and reactor cores.

Son, H., Suh, K., 2004. Result of calculations of the standard problem hydraulics and heat transfer in a subassembly model cooled by liquid metal coolant. Hydrodynamics and heat transfer in reactor components cooled by liquid metal coolants in single/two-phase 218–237.

Teschendorff, V., Austregesilo, H., Lerchl, G., 1997. Methodology, status and plans for development and assessment of the code ATHLET.

Yoon, H.Y., Lee, J.R., Kim, HYUNGRAE, Park, IK.K., Song, CHUL.-HWA., Cho, H.K., Jeong, J.J., 2014. Recent improvements in the CUPID code for a multi-dimensional two-phase flow analysis of nuclear reactor components. Nuclear Engineering and Technology 46 (5), 655–666.

Zhukov, A., Sorokin, A., Smirnov, V., Papandin, M., 1994. Heat transfer in lead cooled fast reactor (LCFR). In: Proceedings of the ARS'94 International Topical Meeting on Advanced Reactors Safety, pp. 66–69.